

Calcic amphiboles of mafic rocks of the Jeffers Brook plutonic complex, Nova Scotia, Canada

GEORGIA PE-PIPER

Department of Geology, St. Mary's University, Halifax, Nova Scotia B3H 3C3, Canada

ABSTRACT

Amphiboles from mafic facies within a Late Proterozoic granodioritic complex pluton show a variety of textures similar to those reported for amphiboles from porphyry-copper granodiorites. Complexly zoned phenocrysts of hornblende have cores of pargasite, clinopyroxene, or actinolite and actinolitic hornblende, and some have rims of actinolitic hornblende. Hornblende shows patchy compositional domains with gradational boundaries and also occurs as crystal aggregates. Actinolite occurs as small euhedral crystals in patches of actinolitic hornblende. Electron-microprobe analyses show clusters of data defining four compositional types of amphibole—pargasite, hornblende, actinolitic hornblende, and actinolite. Of these, actinolite shows coupled substitutions different from those of hornblende and pargasite, and variability in actinolitic hornblende falls on either trend. Early minerals crystallized under conditions of low oxygen fugacity, indicated by low Mg content of amphiboles and common sulfide inclusions. Later minerals crystallized under conditions of increasingly higher oxygen fugacity, indicated by high Mg content of amphiboles and abundance of opaque oxides. There is no evidence that the development of actinolite is associated with a discrete late hydrothermal event; rather, it is the result of subsolidus alteration of clinopyroxene. The development of these amphibole textures appears more dependent on the evolution of volatiles than the chemical composition of the magma.

INTRODUCTION

Geologic setting

The Jeffers Brook pluton is a complex dioritic pluton of Late Proterozoic age in the Avalon terrane of the northern Appalachians (Fig. 1; Pe-Piper and Piper, 1987). The plutonic complex consists mainly of granodiorite with minor quartz diorite and tonalite (IUGS nomenclature of Streckeisen, 1976). All these lithologies contain abundant fine-grained enclaves of quartz diorite, diorite, and gabbro. A few gabbroic and dioritic bodies are found as pods either within or marginal to the pluton.

The Jeffers Brook Pluton shows several similarities to calc-alkaline intrusions that are associated with porphyry-copper deposits and occur above subduction zones, notably in the geochemistry of the predominant granodiorite facies (Table 1), the evidence for a significant role of volatiles, and the detailed mineral assemblages (discussed below). It differs in that the more mafic facies show some alkaline characteristics such as relatively high Ti, Zr, Y, and Nb (Table 1).

The small mafic bodies and inclusions within the Jeffers Brook granodiorite contain distinctive amphibole assemblages. This study describes the textural relationships and chemistry of co-existing calcic amphiboles present in six samples from these minor gabbro and diorite facies within the Jeffers Brook pluton.

Origin of complex amphiboles in subalkaline intrusions

Amphiboles similar to those identified in the Jeffers Brook pluton have been described from a number of plutons associated with porphyry-copper mineralization. In a detailed study of the Koloula Igneous Complex in the Solomon Islands, Chivas (1981) identified two types of poorly zoned amphibole: a hornblende and an actinolitic hornblende associated with magnetite. The amphiboles did not show any regular core to rim zoning (except that the outermost rim in some crystals was actinolitic hornblende). Most of the crystals contained patchy domains with compositions ranging from hornblende to actinolite, but with a general trend of increasing Mg content as crystallization progressed. Similar patchy domains were first described by Czamanske and Wones (1973) and have also been reported by Mason (1978) and Hendry et al. (1985). Chivas (1981) and Hendry et al. (1985) showed that there was a general lack of amphiboles with Si between 7.2 and 7.3. Leake (1978) suggested that igneous amphiboles have a maximum Si of 7.3, and Chivas (1981) and Hendry et al. (1985) proposed that actinolitic hornblende with Si > 7.3 crystallized under subsolidus conditions in the presence of a fluid. These Mg-rich amphiboles were developed under conditions of high oxygen fugacity and were preferentially depleted in elements that partition into "late-magmatic" hydrothermal solutions. Chivas (1981)

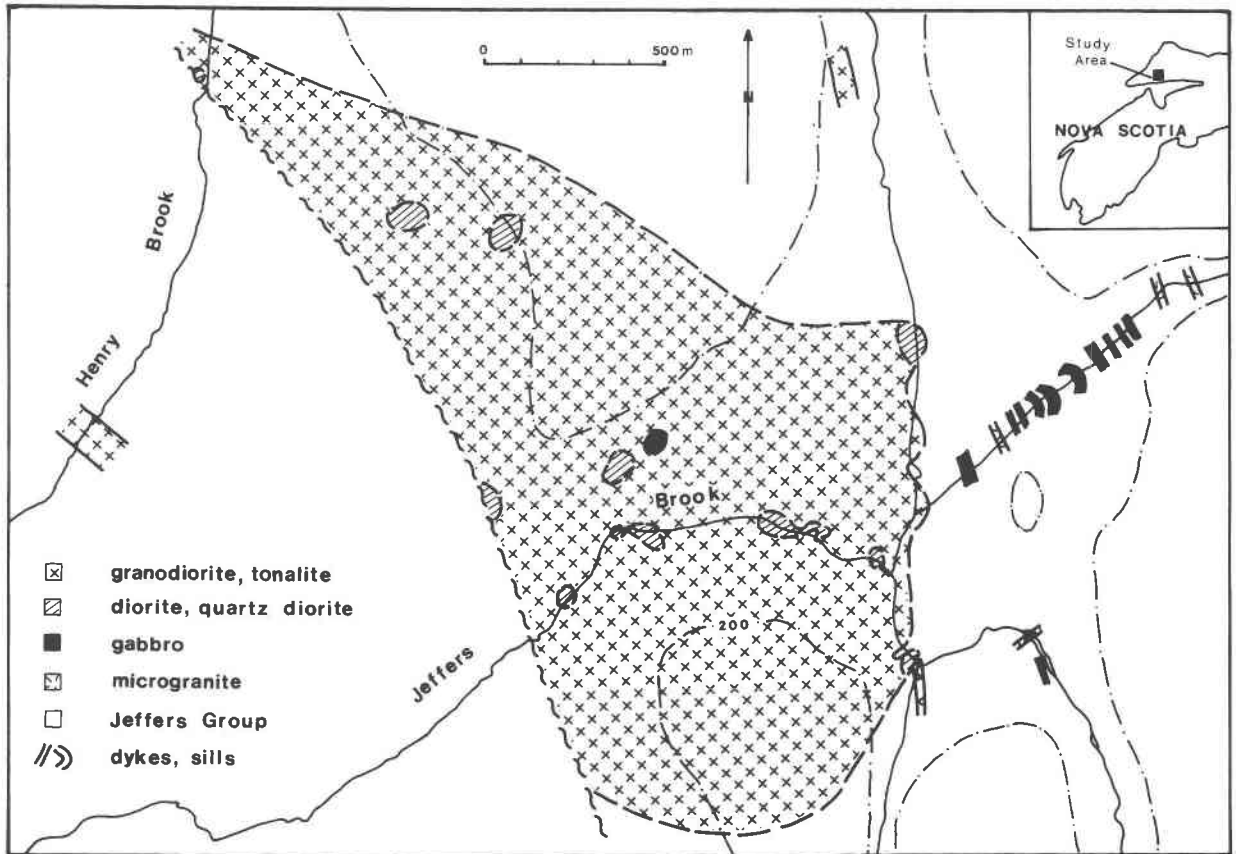


Fig. 1. General geologic map of the Jeffers Brook plutonic complex. Inset shows location in northern Nova Scotia.

found that actinolite occurred as a clear hydrothermal alteration product in most rocks, and from a comparison of mineralized and unmineralized rocks, he proposed that exsolved fluid controlled the degree of oxidation and that amphiboles developed by replacement of pyroxene under subsolidus conditions in the presence of this "late-magmatic" exsolved fluid. In contrast, in a calc-alkaline quartz diorite, Yamaguchi (1985) identified late-magmatic hornblende that showed continuous compositional zoning from hornblende ($Si = 7.24$) to actinolite ($Si = 7.6$) with an outer rim of ferro-actinolitic hornblende composition. The data of Chivas (1981) from Koloula and Hendry et al. (1985) from Christmas, Arizona, also showed continuous compositional trends from hornblende to actinolite when various elements were plotted against Si ; one exception was Mn at Koloula, which reached a maximum in actinolitic hornblende.

Studies of actinolites and hornblendes principally in metamorphic rocks have shown a compositional gap under conditions below the amphibolite facies (Robinson et al., 1982), interpreted by some authors as defining a solvus in the actinolite-hornblende system and by others as a disequilibrium feature. The present study provides no new insights into the definition of the solvus in the hornblende-actinolite system.

With the exception of limited data in Chivas (1981), the studies of igneous rocks cited above investigated am-

phiboles in granodiorites. In the present study, the rocks investigated are gabbros and diorites. Furthermore, they show some alkaline chemical characteristics, in contrast to the calc-alkaline rocks described by previous authors (compare with chemical analyses given by Mason and McDonald, 1978). They thus provide a different set of information on the origin of these amphiboles.

Some of the outstanding questions concerning the amphiboles that are addressed in this study are as follows: (1) Are distinctive hornblende-actinolite relationships of the type described from calc-alkaline granodiorites also found in more alkaline mafic rocks? (2) What are the conditions under which more Mg-rich calcic amphibole forms; in particular, is actinolite a result of later hydrothermal activity, and are actinolitic hornblende and (magnesian) hornblende the result of subsolidus alteration, as proposed by Chivas (1981)? (3) Is $Si = 7.3$ the limit of igneous hornblende, and is there a compositional gap for $Si > 7.2$? (4) Is there evidence from chemical analyses of coexisting amphiboles for the nature of this compositional gap? (5) Is there continuous chemical variation from hornblende through actinolitic hornblende to actinolite?

Methods

The Jeffers Brook pluton was mapped in the field in order to establish the distribution of the major rock facies. Thin sections were studied from a large number of outcrops. This mineralog-

TABLE 1. Representative chemical analyses of major rock facies in the Jeffers Brook pluton

Sample:	1964	1950	3588	1807	1993	2106
SiO ₂	43.90	48.26	49.74	52.40	54.30	63.90
TiO ₂	2.24	1.18	2.80	1.14	1.11	0.54
Al ₂ O ₃	17.50	19.20	13.44	18.20	17.70	16.30
(Fe ₂ O ₃) _{tot}	13.10	9.16	12.78	10.10	8.68	5.08
MnO	0.24	0.20	0.29	0.19	0.23	0.13
MgO	6.81	6.19	5.28	3.55	3.55	1.87
CaO	9.08	8.25	8.79	6.65	6.55	4.46
Na ₂ O	2.28	2.57	2.13	3.82	3.80	4.34
K ₂ O	1.66	2.17	1.52	1.69	1.58	1.64
P ₂ O ₅	0.12	0.19	0.44	0.30	0.25	0.17
L.O.I.	1.85	2.23	1.70	1.85	1.62	1.16
Total	98.78	99.60	98.91	99.89	99.37	99.59
Ba	463	491	459	577	526	615
Rb	62	85	40	56	62	45
Sr	447	363	277	441	486	372
Y	22	20	49	34	26	20
Zr	60	78	286	164	70	126
Nb	7	9	16	15	9	8
Th	1	1	3	3	4	5
Pb	8	40	0	7	15	8
Ga	18	18	24	16	20	15
Zn	89	243	140	82	83	44
Cu	82	38	46	41	22	6
Ni	18	23	42	9	10	9
V	477	266	351	169	161	69
Cr	2	32	84	15	28	34
La	8.30	11.50	n.d.	n.d.	22.80	18.00
Ce	20.00	27.00	n.d.	n.d.	40.00	40.00
Nd	15.00	15.00	n.d.	n.d.	18.00	15.00
Sm	3.54	2.93	n.d.	n.d.	4.82	4.31
Eu	1.36	0.97	n.d.	n.d.	1.69	1.59
Tb	0.50	0.50	n.d.	n.d.	1.10	0.60
Yb	1.63	1.56	n.d.	n.d.	2.37	2.40
Lu	0.28	0.27	n.d.	n.d.	0.42	0.45

Note: Samples are as follows: 1964—hornblende pegmatite vein from eastern margin of pluton; 1950—diorite from western margin of pluton; 3588—Gabbro from western margin of pluton; 1807—diorite from north-west margin of pluton; 1993—quartz diorite from central part of pluton; 2106—typical main granodiorite phase of pluton.

ical study is based on detailed examination of six representative samples. Mineral analyses were made with a JEOL-733 electron microprobe with four wavelength spectrometers and a Tracor Northern 145-eV energy-dispersive detector. Operating conditions were 15 kV at 5-nA beam current. Geological standards were used. Data were reduced using a Tracor Northern ZAF matrix correction program.

PETROGRAPHY

In this study, approximately 40 amphibole-bearing samples were examined from diorite, quartz diorite, a hornblende pegmatite, and diorite inclusions and enclaves. Representative chemical analyses of the host rocks are presented in Table 1. Textural relations between different amphiboles have been studied optically. From these, six representative samples have been selected for detailed mineral-chemistry analysis. In thin section, the diorites (represented by samples C1112, C1950, C1965, C1995) show a hypidiomorphic granular (subophitic) texture and consist of feldspars (60–65%), amphiboles (25–30%), biotite (2–10%), opaques (principally ilmenite and magnetite) (1–5%), and accessory apatite and zircon. They may also contain epidote and chlorite (0–2%). Some of the plagioclase is zoned, and it shows a quite variable

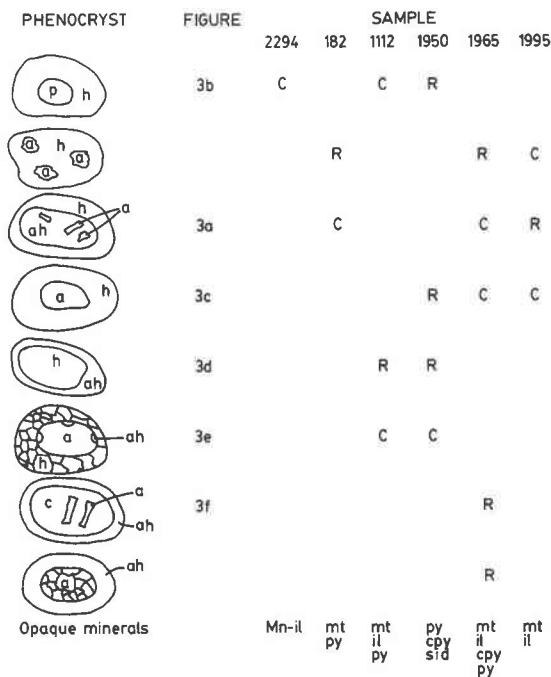


Fig. 2. Cartoon showing schematically the different textural relationships in amphibole phenocrysts (p = pargasite; h = hornblende; ah = actinolitic hornblende; a = actinolite; c = clinopyroxene); the figures in which each of these phenocrysts is illustrated; the abundance of each type in representative samples (C = common, R = rare, otherwise absent); and opaque mineral phases present in the representative samples.

degree of alteration to sericite. Some cores appear highly altered, but many crystals have very fresh rims. Clinopyroxene has been found in only a few samples (represented by C1965). Quartz, if present, appears to have been the last mineral to crystallize, forming either rather patternless intergrowths with the feldspar or filling embayments (possibly due to corrosion) in the plagioclase laths. One sample examined (C1950) contains distinctive large grains of amphibole (described below); this sample contains only trace amounts of opaque minerals.

The quartz diorites (represented by sample C182) show a coarse-grained hypidiomorphic texture and consist of plagioclase (55–70%), amphibole (20–30%), biotite (1–10%), opaques (1–2%), quartz (1–5%), K-feldspar (~2%), and accessory apatite and zircon. Occasional chlorite is present.

The hornblende pegmatite (sample C2294) is coarse grained with a subophitic texture produced by partial inclusion of feldspar in hornblende. Plagioclase (50%), amphibole (35%), quartz (5%), K-feldspar (5%), and accessory sphene and opaques are present. Small amounts of chlorite, epidote, and calcite are present in some samples.

Amphiboles

Description. The following amphiboles (using the nomenclature of Leake, 1978) can be optically distinguished primarily on the basis of color and pleochroism: actinolite, actinolitic hornblende, (magnesian-) hornblende, and

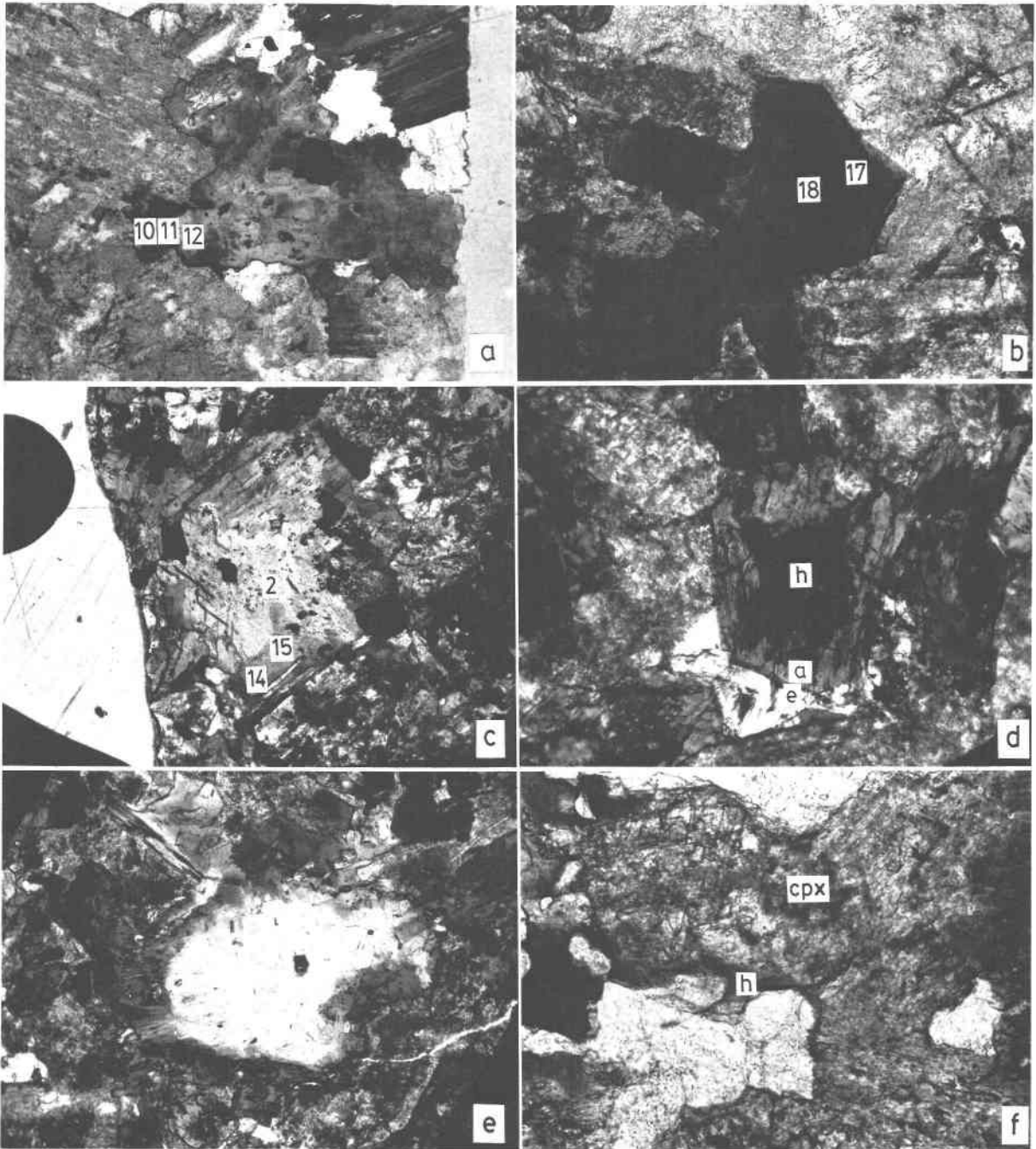


Fig. 3. Photomicrographs showing textural relationships of amphiboles in mafic rocks of the Jeffers Brook pluton. Numbers indicate analyses in Table 2. Abbreviations as in Fig. 2, e = epidote. (a) Subhedral hornblende crystal with an inhomogeneous core made up mainly of actinolite and some patches of actinolitic hornblende. Sample C182. Plane-polarized light; field of view approx. 2.7 mm. (b) Zoned amphibole crystal with green-brown pargasite core and green hornblende margin. Sample C1112. Plane-polarized light; field of view approx. 1 mm. (c) Hornblende crystal with an inhomogeneous core made up primarily of actinolite with some patches of actinolitic hornblende. Sample C1965. Plane-

polarized light; field of view approx. 2.7 mm. (d) Hornblende crystal with rim of actinolitic hornblende and interstitial epidote. Specimen C1112. Plane-polarized light; field of view approx. 1 mm. (e) Colorless to very pale green actinolite prisms or laths, with occasional Fe-Ti oxide grains, overgrown by discrete grains of hornblende. Crystals of actinolitic hornblende occur at the margin of the actinolite core and in the hornblende rim. Sample C1950. Plane-polarized light; field of view approx. 2.7 mm. (f) Clinopyroxene crystal overgrown by hornblende, with actinolite prisms developing at the expense of clinopyroxene. Sample 1965. Plane-polarized light; field of view approx. 1.08 mm.

pargasite. The hornblende is pleochroic dark green to olive-green or yellowish. Actinolite is slightly pleochroic from pale green to colorless, and the actinolitic hornblende is pleochroic from pale blue-green to green. The pargasite is pleochroic dark brown to yellowish-brown. These optically distinct groups also show chemical differences, discussed in more detail below. The correlation between weight percent alumina and the amphibole types can be generalized as follows: actinolite 0.5–3.5%; actinolitic hornblende 3.7–4.7%; hornblende 5.0–10.0%; and pargasite >10%.

In the hornblende pegmatite (C2294), anhedral pargasite cores are in sharp contact with green hornblende rims (Figs. 2, 3b). The hornblende rims are homogenous except that they show a slight zoning to higher Mg content toward the margin. The amphibole crystals in this rock appear fragmented, with secondary chlorite along the fractures and the edges of the grains. There is no trace of actinolite along these fractures. Opaque oxides (manganiferous ilmenite) are rare in this sample.

In the quartz diorites (sample C182), amphibole phenocrysts generally have a poikilitic texture and comprise euhedral to subhedral hornblende with irregular actinolitic patches (Fig. 2), similar to the patchy domains described by Czamanske and Wones (1973). In a few crystals, cores with irregular patches of actinolitic hornblende and euhedral prisms of actinolite are in sharp but irregular contact with homogeneous hornblende rims (Fig. 3a). The sharp, euhedral boundaries of this actinolite differ from those in the patchy actinolite domains in hornblende.

In the diorites, hornblende occurs both as phenocrysts and microphenocrysts. Some of the phenocrysts show a systematic zoning with pargasite cores in sharp contact with homogeneous or slightly zoned hornblende rims (Fig. 3b). The cores of other phenocrysts consist of actinolite prisms (Fig. 3c), in some cases also with patches of actinolitic hornblende and hornblende. In sample C1112, phenocrysts of homogeneous, slightly zoned hornblende are rimmed by a discrete zone of actinolitic hornblende (Fig. 3d). In some samples (e.g., C1112), actinolite also forms aggregates of subhedral microphenocrysts and fills interstices between discrete hornblende phenocrysts. Titanomagnetite is common in these diorites, but appears to be a late-crystallized mineral.

One diorite sample (C1950; Figs. 3e and 4) contains large composite amphibole grains, in which a core of actinolite is rimmed by a number of discrete grains of hornblende, actinolitic hornblende, and rare pargasitic hornblende. The sharp boundaries between the hornblende grains differ from those of the patchy domains described by Czamanske and Wones (1973). The actinolite in the core forms small euhedral to subhedral prisms or laths with occasional sulfide inclusions. Crystals of actinolitic hornblende are also found toward the margin of the actinolite cores, and biotite inclusions occur in these crystals. Rare pyrite, chalcopyrite, and siderite are also present in this sample.

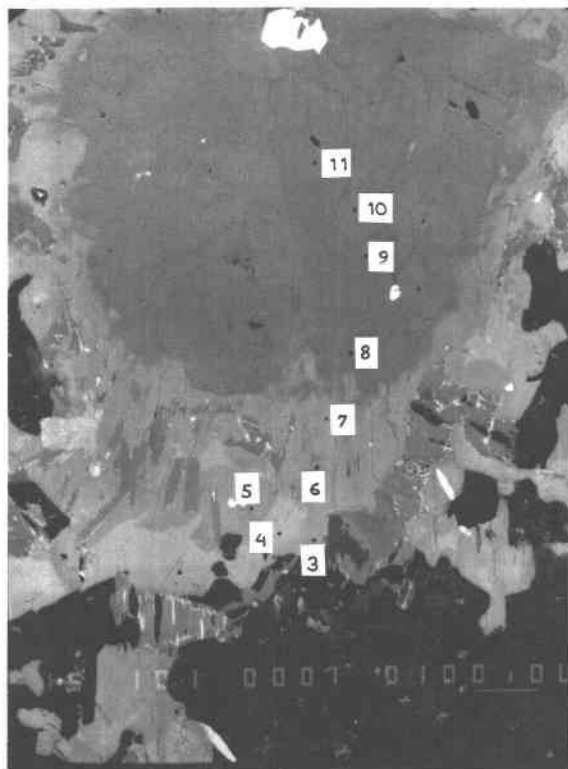


Fig. 4. Backscattered-electron scanning image of part of the same composite grain illustrated in Fig. 3e. Numbered spots indicate analyses in Table 2. Bar is 0.1 mm.

In a few samples (represented by C1965, Fig. 3f), small actinolite prisms are found in clinopyroxene phenocrysts that are rimmed by actinolitic hornblende. These rocks also contain clinopyroxene microphenocrysts and small numbers of actinolitic hornblende microlites.

Interpretation. Individual composite phenocrysts show a range of amphibole compositions, from pargasite to actinolite. In many cases, phenocrysts have cores with sharp contacts with rims of different composition. Cores consist of clinopyroxene, pargasite, actinolite, and small crystals of actinolite within actinolitic hornblende. Patchy compositional domains in phenocrysts are similar to those reported from granodiorites at Finnmarka (Czamanske and Wones, 1973), Koloula (Chivas, 1981), and Christmas (Hendry et al., 1985). The complex amphiboles with distinct cores of actinolite are similar to those described from Koloula gabbros and diorites by Chivas (1981), where the presence of actinolite was believed to be associated with late hydrothermal veining.

Textural data is typically difficult to interpret unequivocally. Euhedral to subhedral homogeneous or zoned crystals are taken to indicate magmatic crystallization. Rims of discrete crystals on phenocrysts generally indicate a reaction relationship with the melt. Subsolidus exsolution generally results in discrete exsolution lamellae. Patchy domains in amphiboles appear to result from subsolidus reactions in the presence of exsolved fluids

TABLE 2. Chemical analyses and structural formulae of representative microprobe analyses of amphiboles from the Jeffers Brook pluton

	182-10	182-11	182-12	1112-17	1112-18	1112-11	1112-8	1112-6	1965-14	1965-15	1965-2
SiO ₂	47.95	48.55	54.79	47.51	42.99	46.98	48.49	52.92	48.65	51.05	54.93
TiO ₂	1.01	1.00	0.13	1.06	2.55	1.04	0.71	0.25	1.01	0.46	0.02
Al ₂ O ₃	6.44	5.95	1.22	7.57	11.35	8.17	6.65	2.92	6.35	4.58	0.67
FeO _{tot}	14.91	14.47	10.98	15.26	16.58	15.88	14.47	13.05	13.95	12.72	12.68
MnO	0.48	0.41	0.38	0.39	0.38	0.40	0.36	0.50	0.38	0.43	0.32
MgO	12.63	12.74	16.33	12.69	10.74	12.55	13.85	16.61	13.22	14.39	14.83
CaO	12.22	12.71	13.07	11.96	11.55	11.97	12.17	11.42	12.03	11.99	13.98
Na ₂ O	0.97	0.74	0.20	1.03	1.68	1.10	0.92	0.45	1.02	0.69	0.04
K ₂ O	0.47	0.50	0.03	0.32	0.44	0.38	0.08	0.06	0.32	0.06	—
Total	97.08	97.06	97.13	97.79	98.25	98.38	97.70	98.16	96.94	96.36	97.46
Structural formulae based on O = 23											
Si	7.099	7.188	7.894	6.952	6.355	6.840	7.038	7.497	7.165	7.469	7.998
Ti	0.112	0.111	0.014	0.117	0.283	0.114	0.078	0.027	0.112	0.051	0.002
^{iv} Al	0.901	0.812	0.106	1.048	1.645	1.160	0.962	0.488	0.835	0.531	0.002
^{vi} Al	0.223	0.227	0.101	0.258	0.333	0.242	0.176	—	0.268	0.259	0.113
Fe ³⁺	0.157	0.039	—	0.349	0.376	0.465	0.485	0.625	0.104	0.096	—
Fe ²⁺	1.689	1.752	1.323	1.519	1.674	1.468	1.271	0.921	1.615	1.460	1.544
Mn	0.060	0.051	0.046	0.048	0.048	0.049	0.044	0.060	0.047	0.053	0.039
Mg	2.787	2.811	3.507	2.767	2.366	2.723	2.996	3.507	2.902	3.137	3.218
Ca	1.939	2.016	2.018	1.875	1.829	1.867	1.893	1.734	1.899	1.880	2.181
Na	0.278	0.212	0.056	0.292	0.482	0.311	0.259	0.124	0.291	0.196	0.011
K	0.089	0.094	0.006	0.060	0.083	0.071	0.015	0.011	0.060	0.011	—
Mg/(Mg + Fe ²⁺)	0.62	0.62	0.71	0.62	0.59	0.65	0.70	0.79	0.64	0.68	0.63
1950-3 1950-4 1950-5 1950-6 1950-7 1950-8 1950-9 1950-10 1950-11 2294-9 2294-7											
SiO ₂	46.95	43.37	48.55	48.35	49.04	54.83	54.84	54.69	55.29	49.25	41.98
TiO ₂	1.05	1.51	0.94	0.82	0.89	0.19	0.21	0.14	0.16	0.88	3.15
Al ₂ O ₃	7.70	10.33	6.53	6.66	5.96	1.38	1.64	0.96	1.17	5.78	12.80
FeO _{tot}	15.75	17.19	14.80	15.77	14.18	11.10	11.21	11.58	11.35	14.85	11.78
MnO	0.32	0.34	0.34	0.46	0.33	0.37	0.32	0.41	0.33	0.58	0.21
MgO	12.48	10.61	13.34	12.88	13.73	17.15	17.18	17.68	17.67	13.65	12.78
CaO	11.59	11.64	11.72	11.16	11.95	11.94	12.13	11.34	11.54	11.84	11.99
Na ₂ O	1.23	1.44	0.95	1.25	0.87	0.30	0.27	0.22	0.32	0.88	2.24
K ₂ O	0.45	0.73	0.51	0.37	0.39	0.06	0.11	0.11	0.07	0.21	0.36
Total	97.52	97.16	97.68	97.72	97.34	97.32	97.91	97.13	97.90	97.92	97.88
Structural formulae based on O = 23											
Si	6.911	6.499	7.094	7.079	7.169	7.817	7.777	7.778	7.808	7.156	6.189
Ti	0.116	0.170	0.103	0.090	0.098	0.020	0.022	0.015	0.017	0.096	0.349
^{iv} Al	1.089	1.501	0.906	0.921	0.831	0.183	0.223	0.161	0.192	0.844	1.811
^{vi} Al	0.247	0.324	0.219	0.229	0.196	0.049	0.051	—	0.003	0.146	0.414
Fe ³⁺	0.369	0.434	0.303	0.366	0.265	0.191	0.204	0.471	0.331	0.399	0.107
Fe ²⁺	1.570	1.720	1.506	1.565	1.469	1.133	1.126	0.906	1.009	1.406	1.345
Mn	0.040	0.043	0.042	0.057	0.041	0.045	0.038	0.049	0.039	0.071	0.026
Mg	2.738	2.370	2.905	2.810	2.991	3.644	3.631	3.747	3.719	2.956	2.808
Ca	1.828	1.869	1.835	1.751	1.871	1.824	1.843	1.728	1.746	1.843	1.894
Na	0.351	0.418	0.269	0.355	0.247	0.083	0.074	0.061	0.088	0.248	0.640
K	0.085	0.140	0.095	0.069	0.073	0.011	0.020	0.020	0.013	0.039	0.068
Mg/(Mg + Fe ²⁺)	0.64	0.58	0.66	0.64	0.67	0.76	0.76	0.81	0.79	0.68	0.68

Note: The positions of these analyses—except 1112-6, 1112-8, 1112-11, 2294-7, and 2294-9—are shown in Figures 3 and 4. The analyses 1112-6, 1112-8, and 1112-11 come from hornblende overgrowths (1112-11) on a core of actinolite prisms (1112-6) with minor actinolitic hornblende and hornblende (1112-8) similar to that illustrated in Fig. 3c. Analysis 2294-7 comes from the brown pargasite core and analysis 2294-9 comes from the green hornblende margin of a zoned phenocryst, similar to that illustrated in Fig. 3b.

(Chivas, 1981). In general, retrograde metamorphism or subsolidus alteration results in chemical disequilibrium and patchy development of minerals. Late-stage circulating hydrothermal fluids are associated with alteration along veins and cracks.

The textural data suggest that pargasite and clinopyroxene were early phases to crystallize, forming the cores to phenocrysts with hornblende or, less commonly, actinolitic hornblende rims. All of these phases appear from their textures to have crystallized under magmatic conditions. Actinolite, or actinolite and actinolitic hornblende, form crystalline aggregates at the expense of clinopyroxene in many phenocrysts. Crystal boundaries are

sharp; patchy compositional domains are not developed, and the textures are typical of subsolidus crystallization. Actinolite also occurs as patchy compositional domains within hornblende phenocrysts and exceptionally is found in the interstices between hornblende crystals. There is no evidence for actinolite resulting from late hydrothermal activity; it is not associated with fractures or veins.

In contrast, the textural evidence suggests that some actinolitic hornblende is of igneous origin, because it occurs as homogeneous rims to hornblende phenocrysts and as microphenocrysts. Actinolitic hornblende also occurs in an apparent subsolidus relationship with actinolite in the cores of phenocrysts.

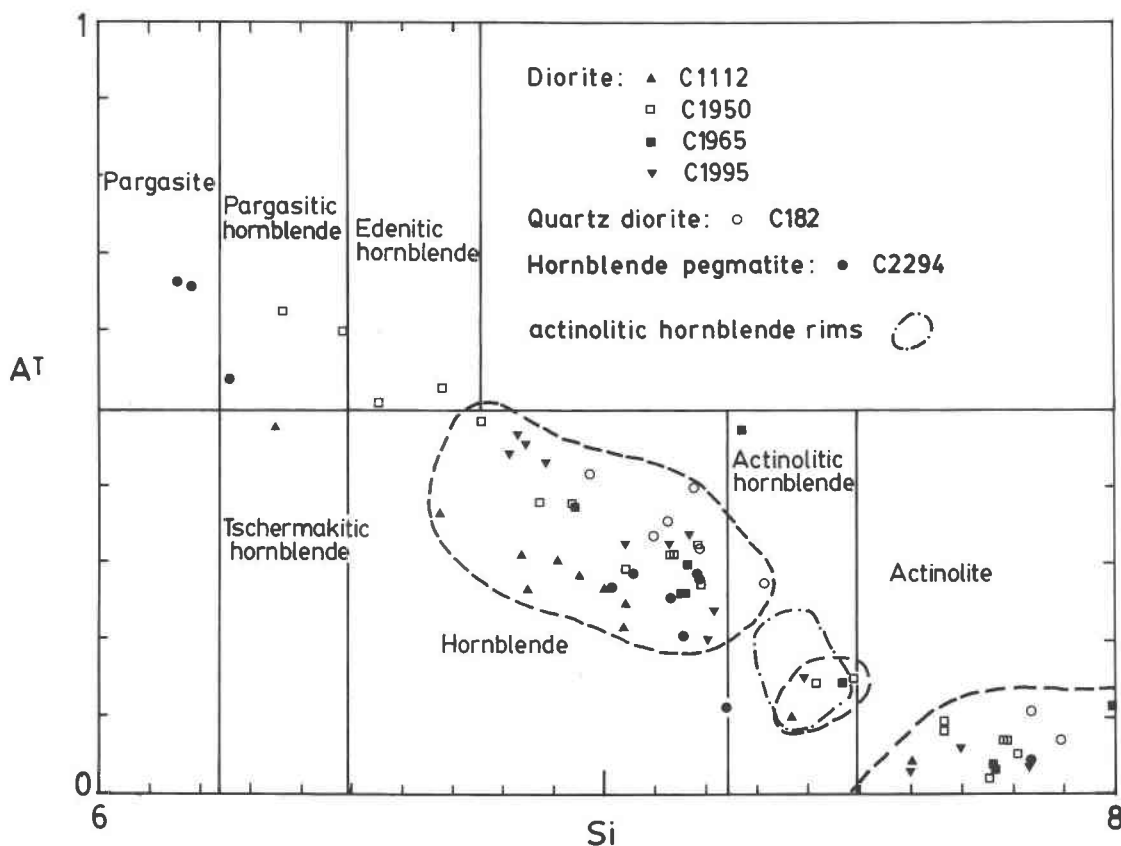


Fig. 5. Plot of $(\text{Na} + \text{K})_{(\text{A})}$ versus Si. Nomenclature according to Leake (1978). Symbols indicate different rock samples. Dashed lines show concentration of samples in the hornblende, actinolitic hornblende, and actinolite fields.

The homogeneous hornblende crystals, which in places have cores of pargasite or actinolite and actinolitic hornblende and have rims of actinolitic hornblende, appear to be of igneous origin. Aggregates of hornblende grains probably resulted from reaction of clinopyroxene phenocrysts with the magma. Hornblende grains with patchy domains of actinolite are similar to those described by Chivas (1981) as resulting from subsolidus reaction with exsolved fluids.

Opaque minerals

Opaque minerals in three samples have been analyzed in detail by electron microprobe (Fig. 2). The clinopyroxene-bearing diorite (sample C1965) contains abundant opaque minerals, both as small independent crystals and as aggregates of similar crystals. Four types of independent crystals are distinguished: magnetite, ilmenite, chalcopyrite, and pyrite. Some of the oxide crystals contain small inclusions of sulfide. The aggregates consist of opaque oxides and sulfide crystals. The textural relationships in this sample suggest that amphibole co-precipitated with the opaque minerals.

The diorite with large amphibole grains (C1950) contains <1% opaque minerals. Small microphenocrysts consist of pyrite, chalcopyrite, siderite (with pyrite inclusions), and composite crystals. The composite crystals are euhedral and contain all three above-mentioned phases,

with the addition of some silicate patches and thin streaks of an unidentified phase. Pyrite, and in some crystals also siderite, occurs as inclusions in the amphibole grains and phenocrysts.

The hornblende pegmatite (quartz diorite, sample C2294) also contains <1% opaque minerals. These occur as small crystals of manganiferous ilmenite, some of which form inclusions in the amphibole. One unusual crystal consisted of a complex mixture of manganiferous ilmenite, rutile, and sphene. It may represent a reaction between ilmenite and exsolved late-magmatic fluid to produce sphene and rutile. Mn appears to replace Fe^{2+} in manganiferous ilmenite, indicating high oxygen fugacity.

The textural relationships in these samples suggest that sulfide minerals (indicating low oxygen fugacity), which occur as inclusions, crystallized early and were followed by oxides (under conditions of higher oxygen fugacity). Magnetite is a common late-crystallizing mineral in samples in which the last amphibole phase is actinolitic hornblende.

CHEMICAL MINERALOGY OF THE AMPHIBOLES

To study the chemical interrelationships among the different amphiboles, chemical analyses of individual minerals were made by electron microprobe. Analyses were screened by rejecting those with totals outside the range 96.5 to 98.5%, yielding a data set of 78 analyses.

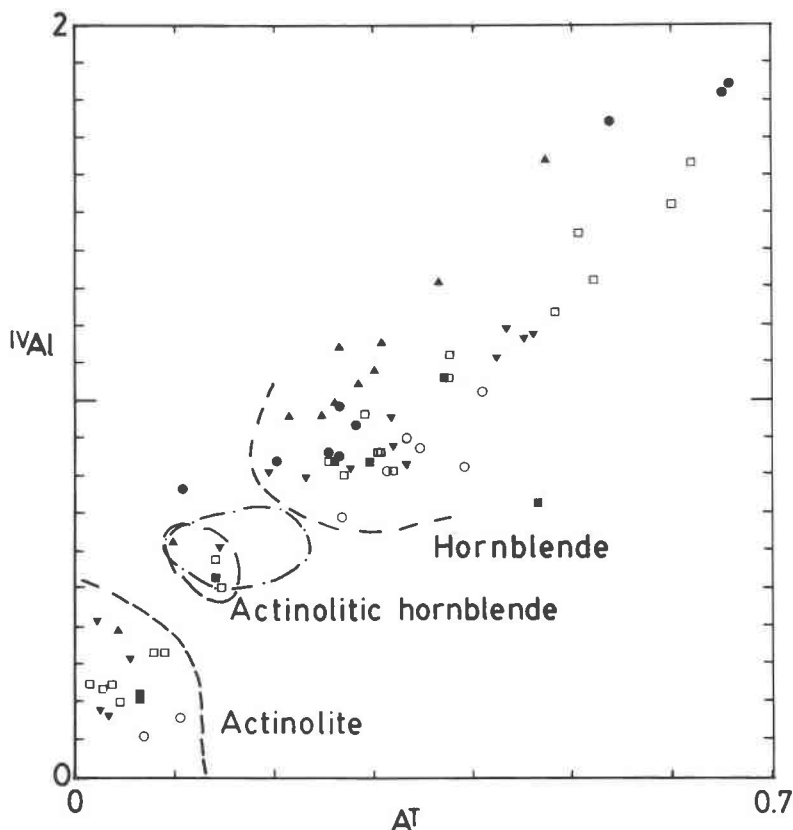


Fig. 6. Plot of ^{IV}Al vs. A-site occupancy, showing compositional gaps between actinolite, actinolitic hornblende, and hornblende. Symbols as in Fig. 5.

Structural formulae have been calculated from microprobe analyses by using crystal-chemical constraints according to the method described by Stout (1972) and Robinson et al. (1982). First, the structural formulae were calculated assuming total cations to be 13, exclusive of K, Na, and Ca. The resulting calculated value for Fe^{3+} is the maximum consistent with stoichiometry. This calculation gave a range of values for Fe^{3+}/Fe_{tot} from 0.12 to 0.39 for actinolite, 0.01 to 0.37 for actinolitic hornblende, and 0.01 to 0.36 for hornblende. Many of these values are unreasonably high. Second, the structural formulae were calculated assuming total cations to be 15, exclusive of K and Na. The resulting calculated value for Fe^{3+} is the minimum consistent with stoichiometry. The average Fe^{3+}/Fe_{tot} ratios range from 0.01 for actinolite to 0.09 for hornblende. These averages are probably a little low. We therefore use the mean values of the two methods of calculation (13 and 15 cations) in discussing the composition of these amphiboles (Table 2).

The chemical classification of these amphiboles is shown in Figure 5. The classification of Leake (1978) has been used throughout this paper, except that the group of similar amphiboles falling in the pargasite, pargasitic hornblende, and tschermakitic hornblende fields are referred to simply as pargasite. Two samples that just fall within the edenitic hornblende field are regarded as hornblende. The plot in Figure 5 also shows that most ana-

lyzed amphiboles cluster in either the hornblende or actinolite fields. There are fewer analyses of pargasite or actinolitic hornblende composition. Actinolitic hornblende analyses show a distinct cluster on plots of Al and Si composition (Figs. 5–11), whereas there is a substantial spread of pargasite analyses.

Amphibole types that have been distinguished optically also cluster into groups on the basis of mineral chemistry. Few chemical analyses fall in the compositional ranges between actinolite, actinolitic hornblende, and hornblende (Figs. 5 and 6), but there is no evidence for an actual compositional gap. Chivas (1981) also found a similar distribution for amphiboles inferred as subsolidus. Yamaguchi (1985) found rapid compositional changes in zoned amphibole in the compositional range of actinolitic hornblende. There is also a paucity of analyses falling between hornblende and pargasite, which is clearly seen in only in variation plots of Mg (Fig. 10) and Al_{tot} (Fig. 11).

Plots (not reproduced here) similar to those in Figures 5 to 11, in which analyses are distinguished on the basis of crystal form (fine and fibrous, coarser and euhedral), show that there are not systematic changes in mineral chemistry between different forms of the same mineral. In particular, there are no systematic differences between fibrous and prismatic actinolite.

All but one of the screened analyses of actinolitic horn-

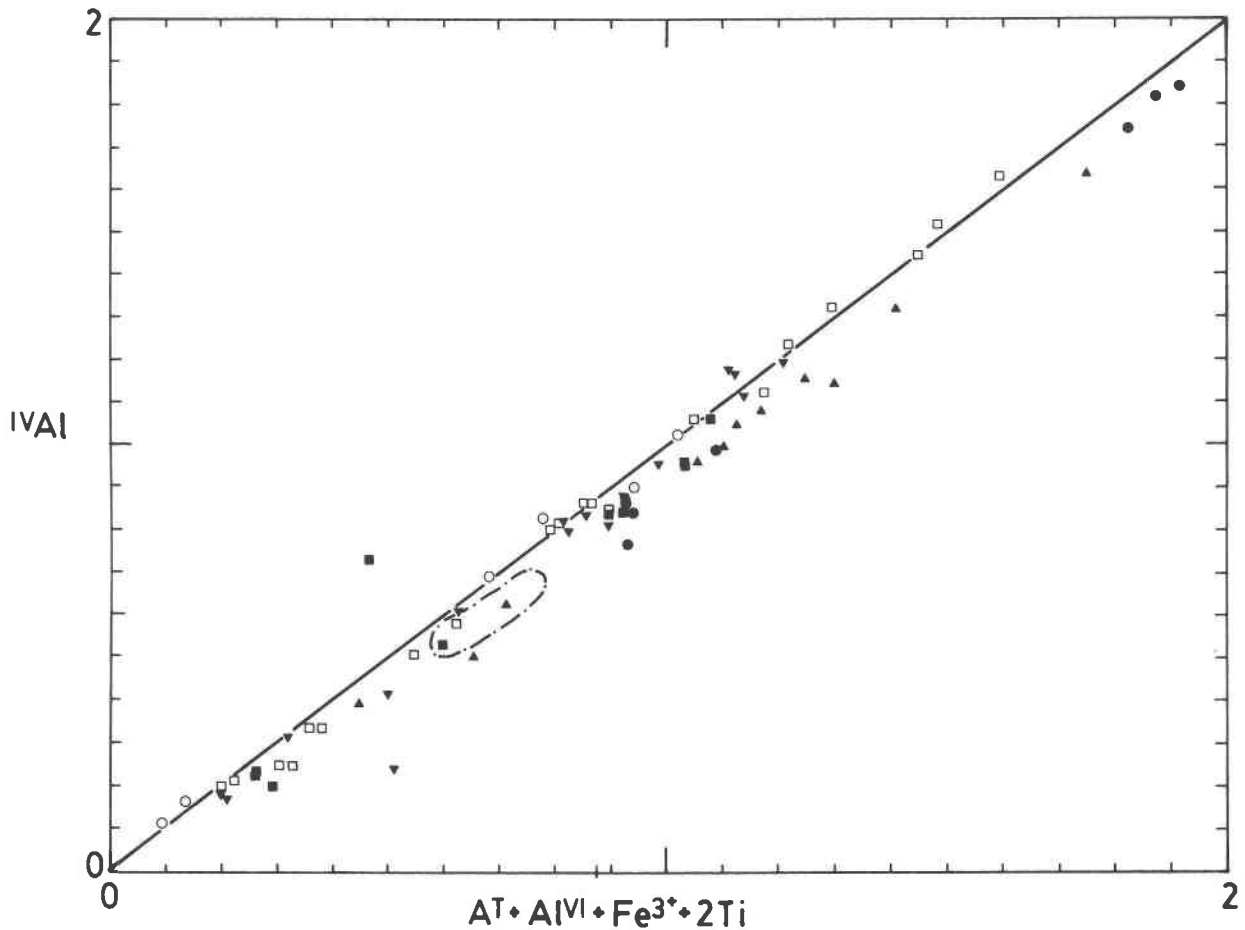


Fig. 7. Plot of $^{[4]}\text{Al}$ against A-site ions + $^{[6]}\text{Al}$ + Fe^{3+} + 2Ti^{4+} . Trend line shows predicted values for perfect substitution. Symbols as in Fig. 5.

blende are from crystals interpreted as subsolidus in origin, i.e., the crystals are either from patchy domains together with hornblende or from cores containing small euhedral actinolite crystals. Other analyses of actinolitic hornblende rims have been screened out because of analytical totals as low as 95.1%. When these analyses are plotted (fields shown in Figs. 5–11), they are indistinguishable from other actinolitic hornblendes. These actinolitic hornblendes show a compositional range similar to the outer parts of zoned hornblende-actinolite crystals described by Yamaguchi (1985). Ferro-actinolitic hornblende of the type described by Yamaguchi was not recognized.

Coupled substitutions

The data presented by Chivas (1981) and Yamaguchi (1985) indicate that there is continuous chemical variation from hornblende through actinolitic hornblende to actinolite. This variation has been studied in the Jeffers Brook pluton samples by examining some of the principal coupled substitutions operative in the calcic amphiboles through the use of binary-element-variation plots (Figs. 7–11) and through comparison of the data of Chivas

(1981) and Yamaguchi (1985), recalculated in the same manner as the analyses in this paper.

Substitution of $^{[4]}\text{Al}$ for Si in tetrahedral sites in all four types of amphibole is dominantly compensated by substitution of $^{[6]}\text{Al}$, Fe^{3+} , and Ti in octahedral sites and partial occupancy of the A sites by Na and K, as illustrated by the linear relationship in Figure 7. The slight deficiency in $^{[4]}\text{Al}$ indicates that the excess A-site and octahedral charge is not completely balanced by the $^{[4]}\text{Al}$ substitution. This excess octahedral and A-site charge might be balanced by substitution of Na for Ca in the M4 sites.

Edenite-type substitutions of $^{[4]}\text{Al}$ plus $(\text{Na} + \text{K})_{\text{A}}$ for Si and A-site vacancy is illustrated in Figure 8 [in which, following Czamanske et al. (1981), richterite-type substitution effects are removed by subtraction of Na_{M4}]. Amphiboles analyzed by Czamanske et al. (1981) showed a 1:1 relation between $^{[4]}\text{Al}$ and A-site - Na_{M4} , with an intercept at about 0.6 $^{[4]}\text{Al}$ for 0.0 A-site - Na_{M4} . Such a trend line describes well the variability in samples C2294 and C1112 and also in samples analyzed by Chivas (1981) and Yamaguchi (1985). Other samples are best described by a trend line with a similar slope, but an intercept of about 0.5 $^{[4]}\text{Al}$. This trend line reflects less coupling with Al^{3+} , Fe^{3+} , and Ti in octahedral sites. Data for actinolite

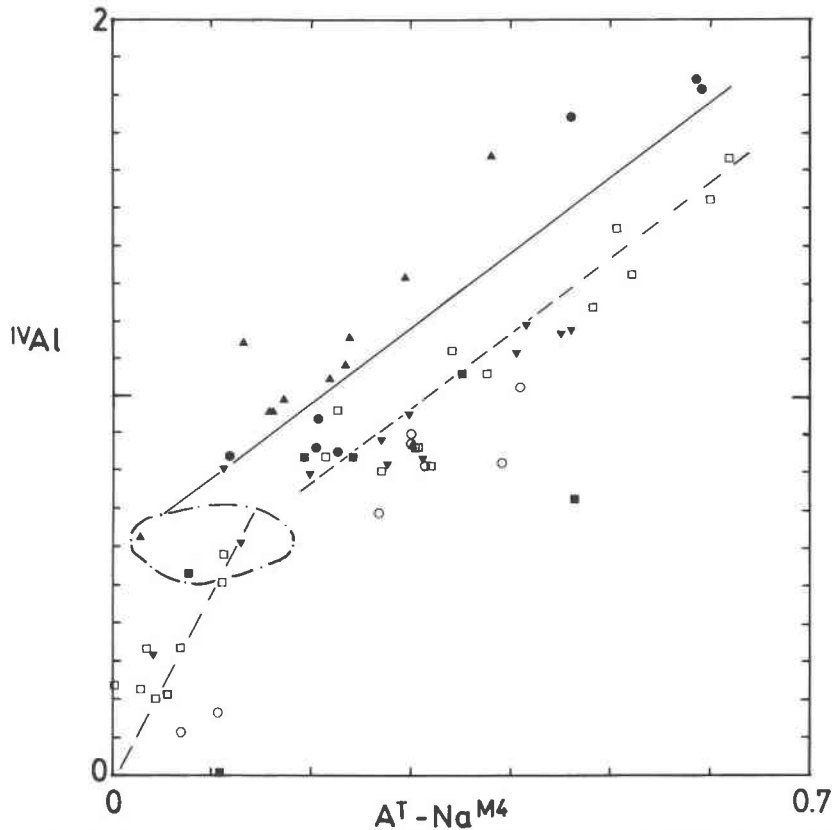


Fig. 8. Plot of ${}^{4}\text{Al}$ against A-site ions $-\text{Na}_{\text{M4}}$. Solid trend line from Czamanske et al. (1981). Dashed lines are trend lines for Jeffers Pluton data discussed in text. Symbols as in Fig. 5.

and actinolitic hornblende show a trend line with a 4:1 relation between ${}^{4}\text{Al}$ and A-site $-\text{Na}_{\text{M4}}$, with an intercept at 0.0 ${}^{4}\text{Al}$.

A plot of ${}^{4}\text{Al}$ against (octahedral) Ti (Fig. 9) likewise shows different trends for actinolite and actinolitic hornblende compared with hornblende and pargasite. For the hornblende, there is a good linear correlation with a ratio of 1:4 and a projected intercept at 0.5 ${}^{4}\text{Al}$ for zero Ti (Fig. 9), similar to the trend found by Czamanske et al. (1981) for Japanese granitoids. The analyses of Chivas (1981) also lie on this trend. Actinolite and actinolitic hornblende, with low ${}^{4}\text{Al}$ and Ti show an indistinct linear trend with a 1:12 ratio passing through the origin. This trend may be in part an artifact of the method of recalculating analyses. Nevertheless, there is only limited coupling of ${}^{4}\text{Al}$ with Ti in actinolite and actinolitic hornblende, which is consistent with the trend shown in Figure 8, in which there is little or no residual of ${}^{4}\text{Al}$ substitution unrelated to A-site occupancy. Samples analyzed by Yamaguchi (1985) contain very low Ti over a wide range of ${}^{4}\text{Al}$ values.

There is only a narrow range of values of $\text{Mg}/(\text{Mg} + \text{Fe}^{2+})$ (total Fe expressed as Fe^{2+}) so that with uncertainties in partitioning Fe, caution must be used in interpreting variations in Mg. There is, however, a strong neg-

ative correlation between Mg and ${}^{4}\text{Al}$ for hornblende, actinolitic hornblende, and actinolite, whereas pargasite shows a positive correlation (Fig. 10). Furthermore, individual zoned crystals of hornblende show an increase in $\text{Mg}/(\text{Mg} + \text{Fe}^{2+})$ from core to rim; such zoning has been interpreted to reflect increasing oxygen fugacity as the magma became more siliceous (Czamanske and Wones, 1973; Yamaguchi, 1985). This indicates that oxygen fugacity may have decreased during the crystallization of the pargasite cores, but increased steadily during the crystallization of hornblende.

The amphiboles described by Chivas (1981) and Yamaguchi (1985) show similar trends of increasing Mg from hornblende to actinolite. Compared to the Jeffers Brook analyses, the igneous amphiboles analyzed by Yamaguchi (1985) have lower Mg content, and the subsolidus amphiboles analyzed by Chivas (1981) have higher Mg content.

In summary, there are clear differences between coupled substitutions occurring in the analyzed samples of actinolite and those occurring in igneous hornblende. There are also differences in some of the coupled substitutions in pargasite. According to the limited data available, there are no differences between subsolvus actinolitic hornblende and that of apparent igneous origin on

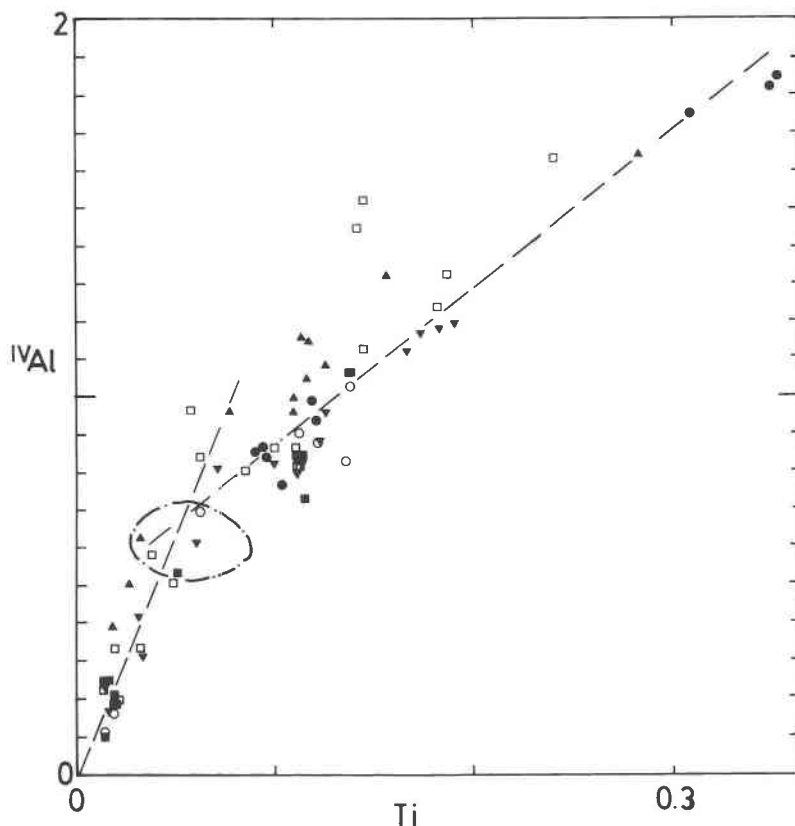


Fig. 9. Plot of ^{14}Al against Ti, showing different 1:4 trend for pargasite and hornblendes and 1:12 trend for actinolite and actinolitic hornblende. Symbols as in Fig. 5.

the rims of phenocrysts. Actinolitic hornblende can be regarded as showing trends that continue those seen in either the hornblendes or the actinolites.

CRYSTALLIZATION HISTORY OF THE AMPHIBOLES

Textural evidence for sequence of crystallization

The overall mineralogy of the pegmatites, diorites, and quartz diorites indicates that magma evolution during crystallization was initially constrained by crystallization of plagioclase and clinopyroxene. The first amphibole to form was pargasite; later, hornblende crystallized. As crystallization proceeded, clinopyroxene became unstable and was replaced by actinolite. Actinolitic hornblende appears to have crystallized on the rims of hornblende grains. The rare actinolitic hornblende microphenocrysts may also be of primary igneous origin. In some samples, the outer parts of zoned phenocrysts are made up of individual hornblende grains; these are presumably reaction products of clinopyroxene with the magma. Patchy domains of actinolite are probably the result of subsolidus reactions in the presence of exsolved fluid.

This inferred crystallization sequence is similar to that identified by Chivas (1981) in the Koulala complex, but with some important differences. In the Jeffers Brook plu-

ton, actinolite (not hornblende and actinolitic hornblende) is the principal product of alteration of clinopyroxene. The textural evidence suggests that most of the hornblende and some of the actinolitic hornblende are the result of magmatic crystallization. Alteration by exsolved late-magmatic fluids, to produce patchy domains, is of limited effect.

It might be questioned whether the actinolitic hornblende rims are of igneous origin. Although their texture supports this interpretation, chemically they are indistinguishable from subsolvus amphiboles and have compositions that many authors regard as beyond the range of igneous amphiboles. Although it might be argued that some other distinct phase crystallized on the rims and was subsequently altered to actinolitic hornblende, such an interpretation cannot be applied to zoned actinolitic hornblende of similar composition recognized by Yamaguchi (1985), which has an outer rim of ferro-actinolitic hornblende.

Pressure conditions of crystallization

Hammarstrom and Zen (1986) have suggested that total Al might be used as a geobarometer in igneous amphiboles. They have demonstrated that there is a linear relationship between ^{14}Al and Al_{tot} for the range $0.5 <$

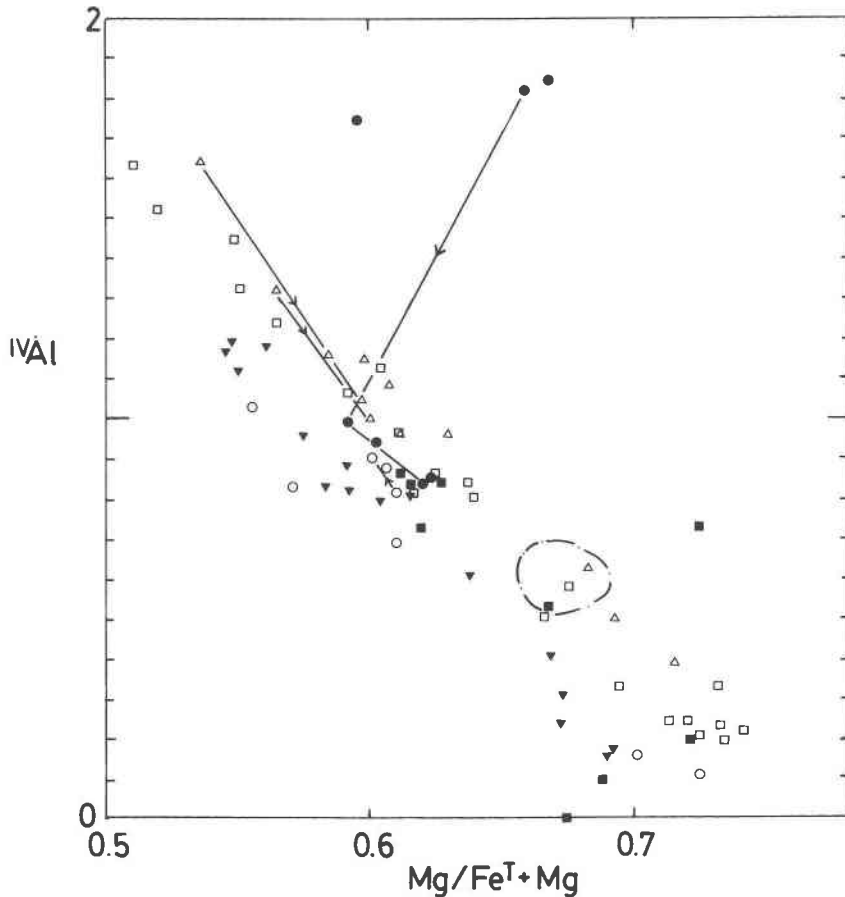


Fig. 10. Plot of ^{41}Al against $\text{Mg}/(\text{Fe}_{\text{tot}} + \text{Mg})$ to show difference in Fe/Mg ratio between actinolite–actinolitic hornblende and hornblende–pargasite. Lines join analyses of inferred igneous amphiboles from the same zoned crystal. Symbols as in Fig. 5.

$\text{Al}_{\text{tot}} < 2.6$. Their calculations were made on the basis of all Fe as FeO and 23 oxygens. A similar plot using chemical mineralogy as determined in this paper is presented in Figure 11, in which their corrected regression line is shown. (The difference between the two estimates of Al composition is less than 4%.) This plot also shows the estimated crystallization pressure based on the Al_{tot} content and the regression equation of Hammarstrom and Zen. This equation is clearly not applicable to the actinolites and actinolitic hornblendes, which show coupled substitutions different from those of the hornblendes and which lie beyond the range of Al compositions investigated by Hammarstrom and Zen. The maximum pressure of about 7 kbar is found for the pargasite in the pegmatite. Hornblende pargasite cores in the diorite suggest pressures of 5–6 kbar, whereas pressures of less than 4 kbar are estimated for the later hornblendes in all rock types.

Oxygen fugacity

The overall paucity of magnetite in diorites such as sample C1950, the absence of magnetite as inclusions in early-formed phenocrysts, and the occurrence of sulfide inclusions in some diorites are evidence of low oxygen

fugacity during the early stages of crystallization. The decrease in Mg content in pargasites also indicates decreasing oxygen fugacity during early crystallization states. However, during late stages of crystallization, there is evidence of higher oxygen fugacity. Ilmenite in the hornblende pegmatite is rich in Mn, and late-stage magnetite (with a high hematite component) appears in most samples. There is a progressive increase in Mg content of hornblendes.

CONCLUSIONS

1. Mineralogical features of amphiboles seen in calc-alkaline granodiorites, such as patchy domains and the abundance of actinolite (Chivas, 1981), are also observed in more mafic alkaline rocks. Distinctive textures include (a) in the hornblende, patchy compositional domains that lack sharp boundaries (similar to the domains described by Czamanske and Wones, 1973), (b) euhedral actinolite crystals in actinolitic hornblende and clinopyroxene cores to amphibole phenocrysts, and (c) outer rims to zoned phenocrysts consisting of discrete crystals of hornblende. Zoned hornblende crystals with sharp rims of actinolitic hornblende are also seen.

2. The first minerals to crystallize were clinopyroxene

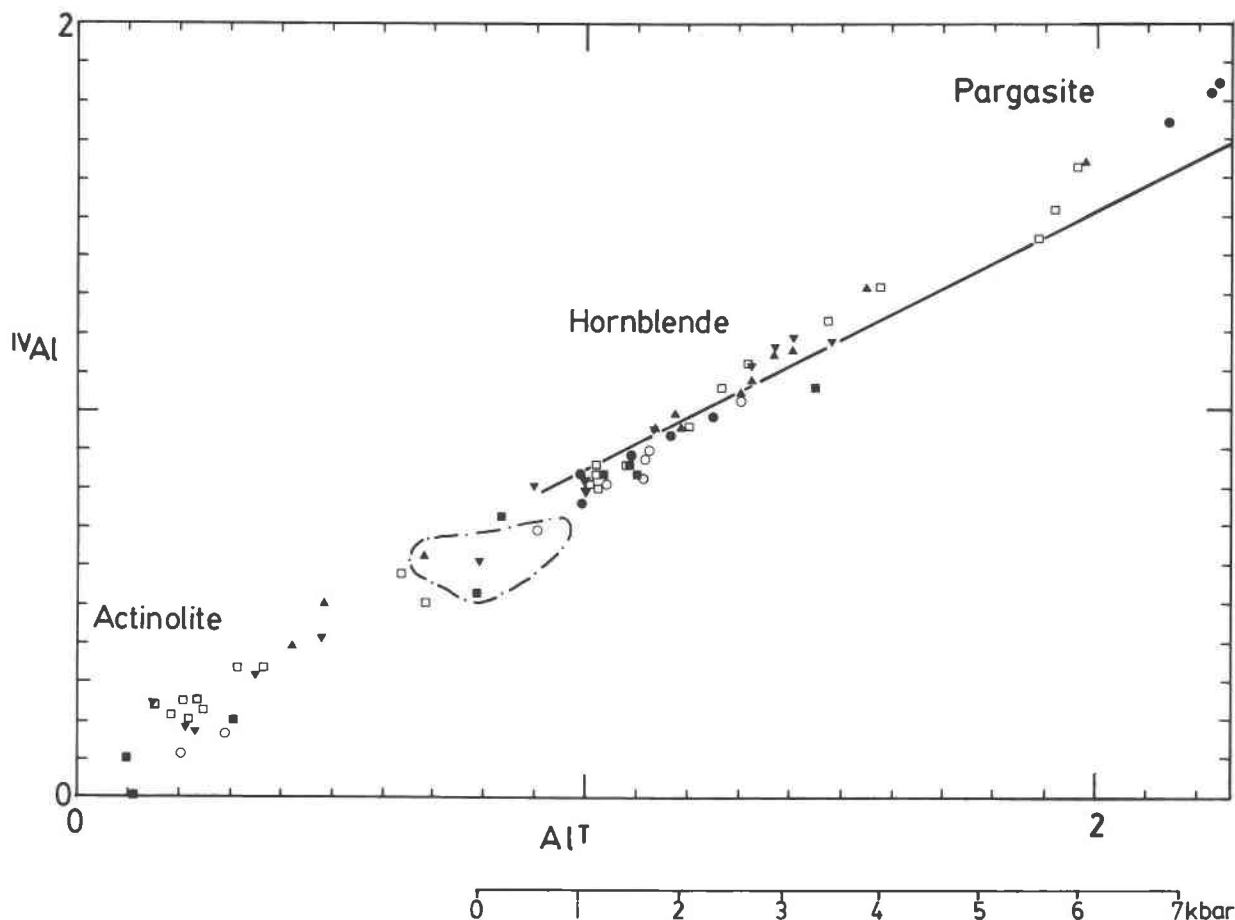


Fig. 11. Plot of Al^t/Al_{tot} vs. Al_{tot} . Reference line from Hammarstrom and Zen (1986), corrected for different method of calculating atomic formulae. Approximate crystallization pressures based on regression equation of Hammarstrom and Zen are also shown for hornblende and pargasite only. Symbols as in Fig. 5.

and pargasite. Hornblende crystallized from the magma on the outer parts of complex phenocrysts. Textures also indicate that hornblende formed by reaction of clinopyroxene with the magma. Actinolite and actinolitic hornblende formed under subsolidus conditions from clinopyroxene. In a few samples, patchy domains of actinolite in hornblende result from subsolidus alteration in the presence of exsolved fluids. Rims of actinolitic hornblende on some phenocrysts appear to be of igneous origin on the basis of their texture.

3. The early-formed minerals crystallized under conditions of low oxygen fugacity (indicated by the presence of sulfides rather than oxides), but later minerals crystallized under conditions of increasingly higher oxygen fugacity (indicated by opaque oxide minerals and the Mg contents of hornblendes). The similarity of the amphibole assemblages in the alkaline diorites studied to those in calc-alkaline granodiorites reported in the literature is probably the result of similar evolution of volatiles in each magma type.

4. There is no textural evidence that actinolite formed from late hydrothermal activity, as proposed by Chivas

(1981). Actinolite has formed by subsolvus alteration of clinopyroxene and possibly other phases. In general, it is absent from cracks and interstices.

5. Chemically, actinolitic hornblende rims of probable igneous origin are indistinguishable from probable subsolvus actinolitic hornblende. Subsolvus actinolites show different coupled substitutions from igneous hornblendes: the actinolitic hornblendes could represent one end member of either of these trends. The actinolitic hornblende rims are of similar chemical composition to igneous actinolitic hornblende described by Yamaguchi (1985). Typical hornblendes have $Si < 7.3$; the actinolitic hornblende rims have $7.3 < Si < 7.6$.

6. Chemical analyses show that there are clusters of analyses centered on compositions corresponding to pargasite, hornblende, actinolitic hornblende, and actinolite, but there are also a few analyses of intermediate composition. At least for the range from hornblende to actinolite, the intermediate analyses between the clusters may indicate rapid changes in composition during magmatic crystallization (as noted by Yamaguchi, 1985), rather than a true compositional gap in the amphiboles.

7. The calcic amphiboles of the Jeffers Brook pluton crystallized at a shallow crustal level at low pressure (mostly less than 4 kbar), but with high partial pressures of water and high oxygen fugacity. One or more of these special conditions may have been responsible for keeping the calcic amphibole solvus at high temperature and thus facilitating the crystallization of actinolitic hornblende under magmatic conditions.

ACKNOWLEDGMENTS

This work was supported by an NSERC operating grant. D. E. Turner and D.J.W. Piper have assisted with this work. Microprobe analyses were carried out at the regional microprobe centre at Dalhousie University. Reviews by F. C. Hawthorne, J. A. Speer, and the journal referees greatly improved the original version of this manuscript.

REFERENCES CITED

- Chivas, A.R. (1981) Geochemical evidence for magmatic fluids in porphyry copper mineralization. Part I. Mafic silicates from the Koloula Igneous Complex. *Contributions to Mineralogy and Petrology*, 78, 389–403.
- Czamanske, G.K., and Wones, D.R. (1973) Oxidation during magmatic differentiation, Finnmarka Complex, Oslo area, Norway: Part 2, The mafic silicates. *Journal of Petrology*, 14, 349–380.
- Czamanske, G.K., Ishihara, S., and Atkin, S.A. (1981) Chemistry of rock-forming minerals of the Cretaceous-Paleogene batholith in southwestern Japan and implications for magma genesis. *Journal of Geophysical Research*, 86, 10431–10469.
- Hammarstrom, J.M., and Zen, E. (1986) Aluminum in hornblende: An empirical igneous geobarometer. *American Mineralogist*, 71, 1297–1313.
- Hendry, D.A.F., Chivas, A.R., Long, J.V.P., and Reed, S.J.B. (1985) Chemical differences between minerals from mineralizing and barren intrusions from some North American porphyry copper deposits. *Contributions to Mineralogy and Petrology*, 89, 317–329.
- Leake, B.E. (1978) Nomenclature of amphiboles. *Mineralogical Magazine*, 42, 533–563.
- Mason, D.R. (1978) Compositional variations in ferromagnesian minerals from porphyry copper-generating and barren intrusions in the Western Highlands, Papua New Guinea. *Economic Geology*, 73, 878–890.
- Mason, D.R., and McDonald, J.A. (1978) Intrusive rocks and porphyry copper occurrences of the Papua New Guinea–Solomon Islands region: A reconnaissance study. *Economic Geology*, 73, 857–877.
- Pe-Piper, G., and Piper, D.J.W. (1987) The pre-Carboniferous rocks of the western Cobequid Hills, Avalon zone, Nova Scotia. *Maritime Sediments and Atlantic Geology*, 23, 41–48.
- Robinson, P., Spear, F.S., Schumacher, J.C., Laird, J., Klein, C., Evans, B.W., and Doolan, B.L. (1982) Phase relations of metamorphic amphiboles: Natural occurrences and theory. *Mineralogical Society of America Reviews in Mineralogy*, 9B, 1–227.
- Stout, J.H. (1972) Phase petrology and mineral chemistry of coexisting amphiboles from Telemark, Norway. *Journal of Petrology*, 13, 99–145.
- Strecheisen, A. (1976) To each plutonic rock its proper name. *Earth-Science Reviews*, 12, 1–33.
- Yamaguchi, Y. (1985) Hornblende-cummingtonite and hornblende-actinolite intergrowths from the Koyama calc-alkaline intrusion, Susa, southwest Japan. *American Mineralogist*, 70, 980–986.

MANUSCRIPT RECEIVED AUGUST 17, 1987

MANUSCRIPT ACCEPTED APRIL 26, 1988